Smart Structures and Systems, *Vol. 22, No. 2 (2018) 185-192*
DOI: https://doi.org/10.12989/sss.2018.22.2.185

Failure prediction of a motor-driven gearbox in a pulverizer under external noise and disturbance

Jungho Park[1], Byungjoo Jeon[1], Jongmin Park[1], Jinshi Cui[2], Myungyon Kim[1] and Byeng D. Youn[*1,2]

[1]*Department of Mechanical and Aerospace Engineering, Seoul National University, 1 Gwanak-ro, Gwanak-gu, Seoul, 08826, Republic of Korea*
[2]*OnePredict. Inc, 1 Gwanak-ro, Gwanak-gu, Seoul, 08826, Republic of Korea*

(Received May 8, 2017, Revised March 15, 2018, Accepted March 19, 2018)

Abstract. Participants in the Asia Pacific Conference of the Prognostics and Health Management Society 2017 (PHMAP 2017) Data Challenge were given measured vibration signals from motor-driven gearboxes used in pulverizers. Using this information, participants were requested to predict failure dates and the faulty components. The measured signals were affected by significant noise and disturbance, as the pulverizers in the provided data worked under actual operating conditions. This paper thus presents a fault prediction method for a motor-driven gearbox in a pulverizer system that can perform under external noise and disturbance conditions. First, two fault features, an RMS value in the higher frequency zones (HRMS) and an amplitude of a period for high-speed shaft in the quefrency domain (QA_{HSS}), were extracted based on frequency analysis using the higher and lower sampling rate data. The two features were then applied to each pulverizer based on results of frequency responses to impact loadings. Then, a regression analysis was used to predict the failure date using the two extracted features. A weighted regression analysis was used to compensate for the imbalance of the features in the given period. In addition, the faulty components in the motor-driven gearboxes were predicted based on the modulated frequency components. The score predicted by the proposed approach was ranked first in the PHMAP 2017 Data Challenge.

Keywords: gearbox; failure prediction; noise; fault diagnosis; prognostics and health management (PHM)

1. Introduction

A gearbox is a critical element found in many mechanical systems. As unexpected failure of a gearbox could lead to a large amount of economic loss, many studies have been conducted to diagnose faults in gearbox systems. Saxena *et al*. (2005) employed Morelet wavelet to extract fault-related characteristics using acceleration signals of a gear used for helicopters. The wavelet techniques could detect the existence of faults under different crack sizes and torque levels. Barszcz and Randall (2009) applied a spectral kurtosis technique to detect a crack in the gear of wind turbines. The method could discover non-Gaussian components in the acceleration signals, and thus detect faulty symptoms of the signals. Other signals like acoustic emission, transmission error, and strain have also been used to detect faults of gear systems (Qu *et al*. 2014, Park *et al*. 2016, Yoon *et al*. 2015). In real-world applications, however, external noise and disturbance exist in the measured signals, and thus uses of the previously described techniques could be limited.

The Asia Pacific Conference of the Prognostics and Health Management Society 2017 (PHMAP 2017) held a data challenge, named the PHMAP 2017 Data Challenge, to address issues surrounding fault diagnosis and prognosis for motor-driven gearboxes in pulverizers. The pulverizers selected are used to grind coal for boilers in the steam generating power cycle. The main purpose of the challenge was to identify (1) the replacement date of the motor-driven gearboxes and (2) the faulty components in the motor-driven gearboxes of the pulverizers. In the challenge, the gearboxes were exposed to significant noise and disturbance because the collected data from the motor-driven gearboxes came from actual operating conditions.

Previous approaches to reduce the effects from noise and disturbance in diagnosis and prognosis of gearboxes were mainly based on time synchronous averaging (TSA) techniques. First, the TSA technique for gears was developed using small sizes of rectangular window functions to isolate vibration signals from the individual gear (McFadden 1991). Later, the rectangular windows were revised into Hann windows to remove discontinuity of the isolated signals (McFadden 1994). In addition, the TSA techniques were improved by using autocorrelation analysis to define the window functions (Ha *et al*. 2016). However, previous TSA-based techniques require angular information that is collected from encoders. Therefore, the techniques involve additional devices and signal processing procedures.

In this challenge, team SHRMer attempted to extract fault-related features of the motor-driven gearboxes under external noise and disturbance using only vibration signals without angular information. From the features, the team

*Corresponding author, Professor
E-mail: bdyoun@snu.ac.kr

ISSN: 1738-1584 (Print), 1738-1991 (Online)

predicted the replacement date and the faulty components. The replacement date can be thought of as the same as the failure date for the purposes of this challenge. To address these issues, this paper is organized as follows. In Section 2, we explain the given challenge problem and data sets. Next, Section 3 provides the analysis results from the given data to reveal the fault-related characteristics of the gearboxes. Then, in Section 4, the failure dates of the pulverizers and the faulty components are predicted by using the fault features. After discussing the results in Section 5, Section 6 concludes this paper with a summary and some suggestions for future work.

2. Problem and data sets

The problem of the PHMAP 2017 Data Challenge is described in Section 2.1. Then, the details of the released data sets and the scoring process are presented in Sections 2.2 and 2.3, respectively.

2.1 Problem definition

The committee of the PHMAP 2017 Data Challenge provided training data sets (Pulverizers C, D, and F), test data sets (Pulverizers A, B, and E), and failure data sets (Failure 1 and 2). Each data set is composed of acceleration, velocity and displacement data. Training and test data sets were irregularly collected for about 2 years, and failure data sets were collected at two instances of 81 and 1 day(s) earlier (Failure 1 and 2, respectively) than the gearbox failure. The ranges of measurement dates are shown in Table 1. The participants in the challenge were asked to predict (1) the replacement date (i.e., failure date) and (2) the faulty component among the motor-driven gearbox components shown in Fig. 1 for the test data sets (i.e., Pulverizers A, B, and E).

2.2 Description of the data sets

The measured data has 4,096 points with different time lengths of 2 or 0.533 seconds. This results in different sampling rates of about 2,048 or 7,680 Hz, respectively. Each measurement was collected from four different points of the pulverizer, Case-1, Case-2, MTR-I_B and MTR-O_B, as shown in Fig. 2.

Table 1 Date range of the data set

Data	Pulverizer	Date Range (YYYY/MM/DD)
Test	A	2011/06/14-2012/07/31
	B	2011/09/08-2013/06/12
	E	2011/06/14-2013/07/31
Training	C	2011/06/14-2013/06/12
	D	2011/06/14-2013/06/12
	F	2011/06/14-2013/06/12
Failure	Failure 1	No information (81 days before failure)
	Failure 2	No information (1 day before failure)

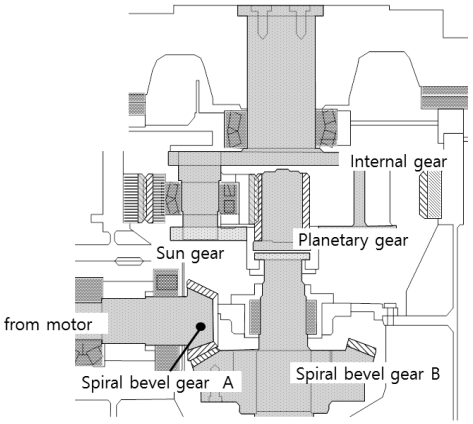

Fig. 1 Detailed components of a motor-driven gearbox in a pulverizer ("PHMAP 2017 Data Challenge", 2017)

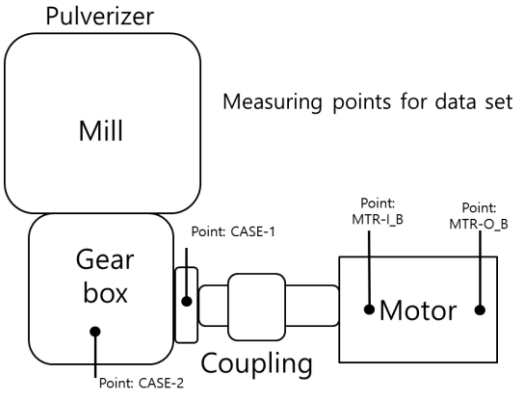

Fig. 2 Measuring points for the data set ("PHMAP 2017 Data Challenge", 2017)

Table 2 Number of gear teeth

Component	Number of teeth
Spiral bevel gear A	15
Spiral bevel gear B	58
Sun gear	15
Planetary gear	33
Internal gear	84

The number of teeth in each gear in the motor-driven gearbox is shown in Table 2, which results in gear ratios of 3.87 and 6.6 at the bevel gear pair and the planetary gear, respectively. Therefore, the total transmission ratio of the system is about 25 times, which reduces the rotating motor speed of 887 rpm to a mill speed 35.1 rpm. Detailed information of the pulverizer system is shown in Table 3. The given data sets include two different operation modes of the pulverizer: idle and loading modes. Idle mode data show relatively low amplitude of vibration; whereas, loading mode data show irregular vibration with high amplitude due to high loads from grinding coal. The detailed analysis about the idle and loading modes are given in Section 3.

Table 3 Gearbox specifications

Weight	120 ton
Motor speed	887 rpm (=14.8 Hz)
Mill speed	35.1 rpm (=0.59 Hz)
Bearing	Sleeve type
Power	448kW

2.3 Scoring process

In the challenge, a scoring function was defined as follows

$$\text{Scoring function} = \sqrt{w_1 \times error_1{}^a + w_2 \times error_2{}^b + w_3 \times error_3{}^c} \quad (1)$$

where $error_1$, $error_2$, and $error_3$ are the differences between the predicted failure dates and the actual failure dates; and w_1, w_2, and w_3 are weighting factors. Weighting factors are 0.7 for a correct answer or 1.0 for a wrong answer for the faulty component of the gearbox. The exponent indices *a*, *b*, and *c* are constants predefined for each team.

3. Data analysis

This section analyzes the characteristic behaviors of the Failure 1 and 2 data compared to normal data measured from the training data sets. In Section 3.1, first, we observe normal and fault data in the time-domain. Then, in Sections 3.2 and 3.3, the normal and fault data are investigated in the frequency domain with sampling rates of 7,680 and 2,048 Hz because data from different sampling rates could give distinct fault characteristics. Next, pulverizers are classified into two groups according to their responses to impact loadings; this is described in Section 3.4.

3.1 Normal and fault signals in the time-domain

Mao and Zhang (2013) found that most failures in motor-driven gearboxes in pulverizers were found at a high-speed gear. In the challenge, therefore, the acceleration signals were used for extracting fault features, as acceleration signals were known to be more efficient in detecting faults of high speed components (Verbruggen, 2003, Shen *et al*. 2014). In addition, the acceleration signals from gearbox Case-1 were used because the location was attached to the high-speed shaft and the location was near the bearing case where accelerometers are usually attached for the purpose of condition monitoring (Caselitz *et al*. 1999, Jung and Koh 2014, Zhu *et al*. 2010).

Fig. 3 shows acceleration signals of normal training data of Pulverizer C from the idle and loading states (from 2011/06/14 and 2011/09/14); and Failure 1 and 2 data measured from gearbox Case-1. In addition, RMS values of the signals are marked. All signals are 0.533-second-long data. As can be seen in Fig. 3, the RMS values are more than four times larger in a loading state than in an idle state, as more loads were transmitted in grinding the coal. However, some impulse signals, which could be evidence of faults in the gear system (McDonald *et al*. 2012), were observed near 0.2 and 0.5 seconds even in a normal idle state. Moreover, normal loading data also have larger amplitudes than fault data which were also measured from loading states. This finding is contradictory to the fact that data from a more degraded gear should have larger RMS values (Lebold *et al*. 2000).

Therefore, we were able to conclude that the pulverizer systems given in this challenge experienced significant noise and disturbance. In this setting, previously developed well-known approaches like wavelet and spectral kurtosis could not be applied.

3.2 Fault features using data from the higher sampling rates

In Sections 3.2 and 3.3, the acceleration signals from normal and faulty pulverizers are compared in the frequency domain. In Section 3.2, first, the comparisons were made using the higher sampling rate data (i.e., 7,680 Hz with 0.533 seconds). It is known that faults of a gearbox will excite the resonance frequency of the system, which is usually located higher than mesh frequency harmonics (Li *et al*. 2016). Therefore, the higher sampling rate made it possible to observe the data in the wider frequency ranges, where fault symptoms could appear.

Fig. 4 shows acceleration signals in the frequency domain between 2,500 and 3,500 Hz in idle and normal loading states; and from Failure 1 and 2 states using the same data in Fig. 3. In the Fig. 4, the largest amplitude values in each state are also marked. We observed that the largest amplitudes in Failure 1 and 2 states are 0.0576 and 0.0932 in the given frequency ranges, while the largest amplitudes in normal idle and normal loading states are 0.0268 and 0.0295. The amplitude shows similar values regardless of whether the pulverizers are in idle or loading states, as shown in Figs. 4(a) and 4(b).

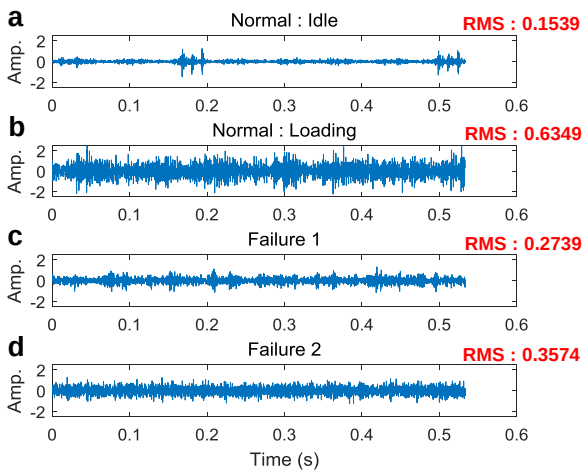

Fig. 3 Time-domain acceleration signals and their corresponding RMS values in (a) normal-idle state, (b) normal-loading state, (c) Failure 1, and (d) Failure 2

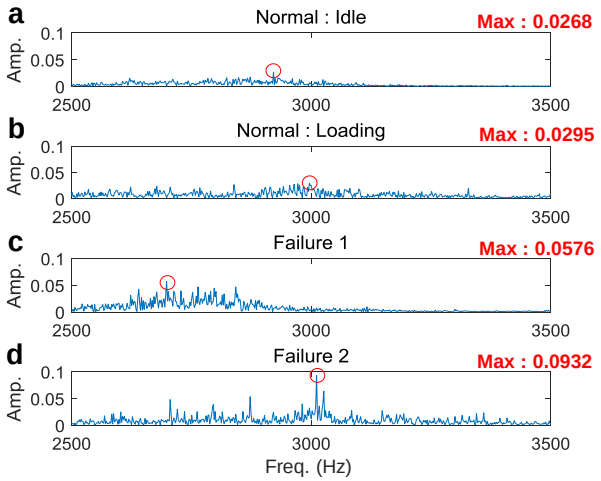

Fig. 4 Frequency-domain acceleration signals with the higher sampling rates (7,680 Hz) between 2,500 and 3,500 Hz and their corresponding maximum amplitudes in (a) normal idle state, (b) normal loading state, (c) Failure 1, and (d) Failure 2

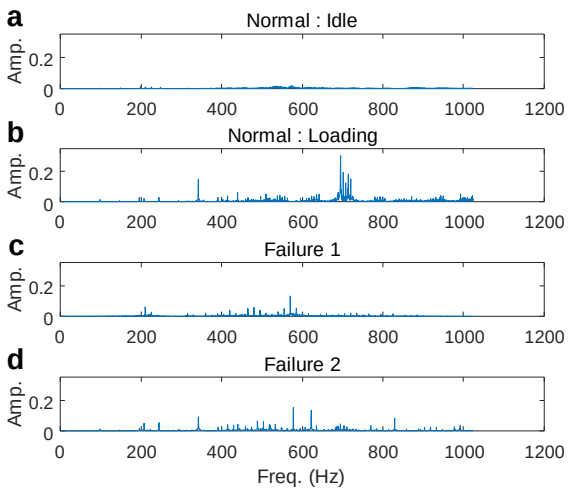

Fig. 5 Frequency-domain acceleration signals with the lower sampling rates (2,048 Hz) between 0 and 1,200 Hz in (a) normal idle state, (b) normal loading state, (c) Failure 1, and (d) Failure 2

In addition, the amplitude shows larger values in Failure 2 (1 day before failure) than in Failure 1 (81 days before failure). From these observations, it is apparent that the energy in the high frequency range (2,500-3,500 Hz) increases as the system degrades. The RMS values for each states are 0.0057, 0.0094, 0.0120, and 0.0124, respectively. From these results, we could know that the characteristics were not affected by loading states or disturbance.

3.3 Fault features using data from the lower sampling rates

In Section 3.3, we compare the acceleration signals of the normal and faulty pulverizers in the frequency domain using the lower sampling rate data (i.e., 2,048 Hz with 2 seconds). Although the lower sampling rate could restrict the available frequency range, the longer measurement time provided a higher resolution of frequency, which makes it possible to observe more detailed frequency-domain behavior.

Fig. 5 shows acceleration signals in the frequency domain between 0 and 1,200 Hz from the idle and normal loading states; and Failure 1 and 2 states using the data from the same date in Figure 3, but with a different sampling rate. As can be seen in Figure 5, the frequency ranges are limited to 1,024 Hz. However, we could observe that periodical peaks appear in Failures 1 and 2, especially between 400 and 600 Hz.

To highlight these periodicities in the frequency domain, we adopted a cepstrum technique, which is defined as "the power spectrum of the logarithm of the power spectrum" (Bogert *et al.* 1963). The technique has been used for fault diagnosis of gearboxes due to its ability to detect modulated sideband components equally spaced in the frequency domain (Randall 2016). Fig. 6 shows the cepstrum analysis results using the same data in Fig. 5. The data were represented in the 'quefrency domain', which is an anagram of the frequency domain. The unit in the quefrency domain is time, and the value in the quefrency domain indicates the period of the components in the frequency domain. We marked the amplitudes when quefrencies are 0.068 seconds, which is the inverse of the high speed shaft frequency, 14.8 Hz.

In Fig. 6, we noticed that the values in Failure 1 and 2 show 0.167 and 0.286, which are larger than the values in idle and normal loading states, 0.079 and 0.096 respectively. In addition, the amplitudes increased gradually from Failure 1 to Failure 2, and idle and loading states could not affect the values more significantly than the existence of faults. From these observations, we determined that the amplitude of the quefrency at the highest shaft speed could differentiate faulty gearboxes from normal ones while representing the degree of degradation of the gearbox.

3.4 Pulverizer classification based on responses to impact loadings

In Section 3.4, we describe how the testing pulverizers were classified into two groups based on their responses to impact loadings. The responses are the criteria to which one of the characteristics extracted in Sections 3.2 and 3.3 is applied.

Fig. 7 shows the time-domain and frequency-domain signals of Pulverizer A on 2012/05/18 and 2012/01/18. The obvious fault-like signals are shown as periodic impulses in time-domain signals in Fig. 7(a), and as excitation in high frequency zones in frequency-domain signals in Fig. 7(b). The impact signals are more significant when compared with data from 2012/01/18 in Figs. 7(c) and 7(d). As faults did not exist in the given measurement period, we could conclude that impact loadings out of the pulverizer systems affected the system, and made fault-like signals on the date 2012/5/18. Fig. 8 shows the largest amplitudes between

2,500 and 3,500 Hz during the given periods for Pulverizers A, B, and E. The dotted and solid red lines are the values from Failure 1 and 2. Then, the shaded areas indicate the periods around 2012/05/18 when impact loadings affected the system. As can be seen, the largest amplitudes of Pulverizer A show a sharp increase on 2012/05/18. The largest amplitudes of Pulverizer B also show an increase on 2012/05/18. On the other hand, the largest amplitudes decrease on 2012/05/18 for Pulverizer E, which indicates that the pulverizer is not sensitive to the impact loadings. In addition, the values from Pulverizer E do not increase gradually, while the ones from Pulverizers A and B increase in the given period.

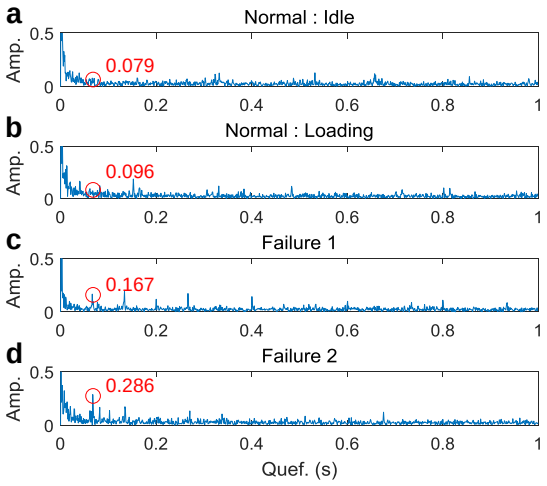

Fig. 6 Quefrency-domain acceleration signals with lower sampling rates between 0 and 1 second and their corresponding amplitudes of the period for the high-speed shaft in (a) normal-idle state, (b) normal-loading state, (c) Failure 1, and (d) Failure 2

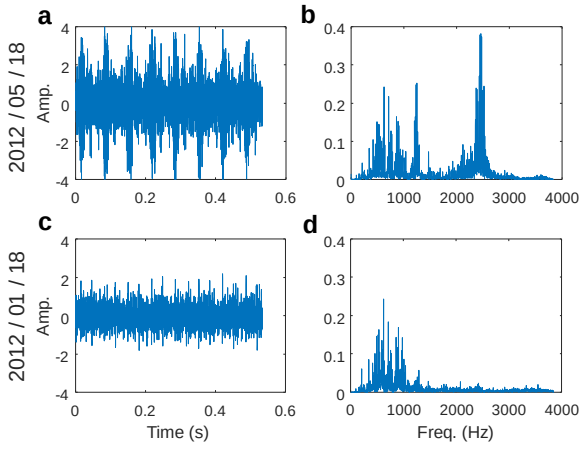

Fig. 7 Acceleration signals from Pulverizer A (a) in the time domain at 2012/05/18, (b) in the frequency domain at 2012/05/18, (c) in the time domain at 2012/01/18, and (d) in the frequency domain at 2012/01/18

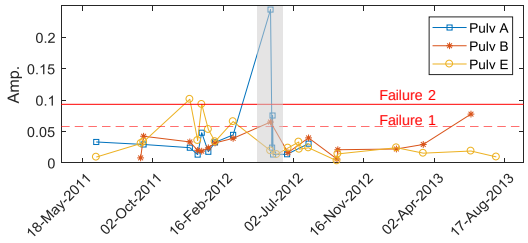

Fig. 8 Maximum amplitude in the higher frequency zone for testing pulverizers (Pulverizers A, B, and E) with Failure 1 and 2 data

As can be seen, each pulverizer had different behaviors as a result of impact loadings. Especially, the responses of Pulverizer E were not significantly affected by the impact loadings compared to Pulverizers A and B. As a result, we could conclude that Pulverizer E had a different characteristic response to impact loadings than did Pulverizers A and B.

4. Failure date and component prediction

In the previous section, two fault characteristics were revealed, and testing pulverizers were classified into two groups based on responses to impact loadings. In Sections 4.1, 4.2, and 4.3, the failure dates are predicted based on physics and data analytics from Section 3. In addition, in Section 4.4, we will discuss the way to predict the faulty components.

4.1 Trends of the fault features in each pulverizer

In this section, two fault features are extracted from testing Pulverizers A, B, and E in the given periods. As explained in Section 3, the amplitudes in the high frequency zones got larger for Pulverizers A and B using higher sampling rates. Therefore, RMS values in the higher frequency zones (HRMS) were calculated to characterize the faulty behaviors in Pulverizers A and B. Then, the amplitudes of periods for the high-speed shaft in the quefrency domain (QA_{HSS}) were calculated from Pulverizer E. The trends of the calculated features are shown in Fig. 9. In extracting the features, the data around 2012/05/18 were not included, because the data from around this date could be deteriorated due to impact loadings out of the system. In the figure, the increases of the features could be observed in the last part of the extracted data, although significant changes were not observed in the first part.

Fig. 10 shows the behaviors of the two features, HRMS and QA_{HSS}, extracted from Pulverizers C, D, and F (training data). As the training pulverizers are under normal degradation, the extracted features showed similar values and did not show significant changes along the given periods.

4.2 Weighted regression

Regression analysis is widely used to predict fault dates

using the sensory signals (Hu *et al*. 2015). Many regression techniques have been developed to make parametric or non-parametric models between input and output data (Wei *et al*. 2015). Among various regression estimation methodologies, this paper implements a weighted regression technique in consideration of imbalance in the given data (Liu and Zio 2017).

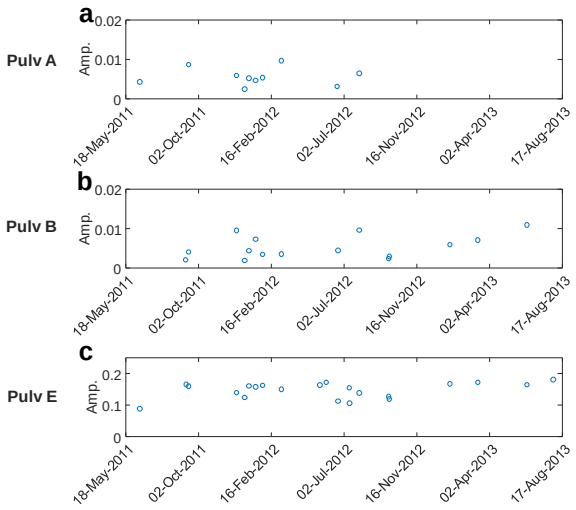

Fig. 9 Trends of the fault features in the test data set: (a) RMS in the higher frequency zone (HRMS) for Pulverizer A, (b) HRMS for Pulverizer B, and (c) amplitudes of the high-speed shaft period in the quefrency domain (QA_{HSS}) for Pulverizer E

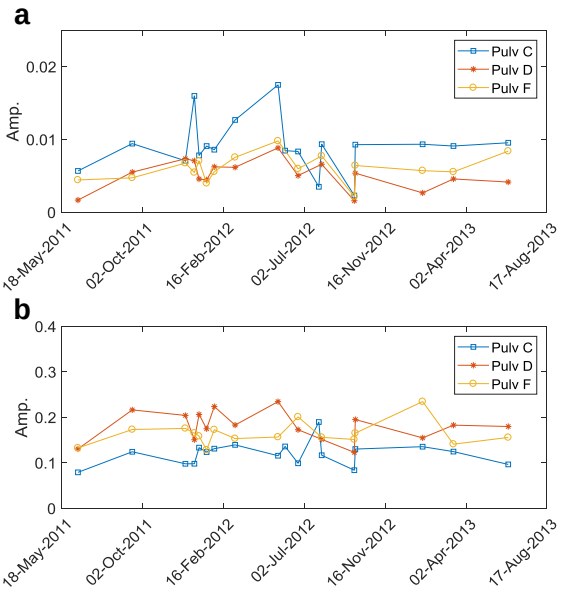

Fig. 10 Trends of the fault features for the training pulverizers (Pulverizers C, D, and F): (a) HRMS and (b) QA_{HSS}

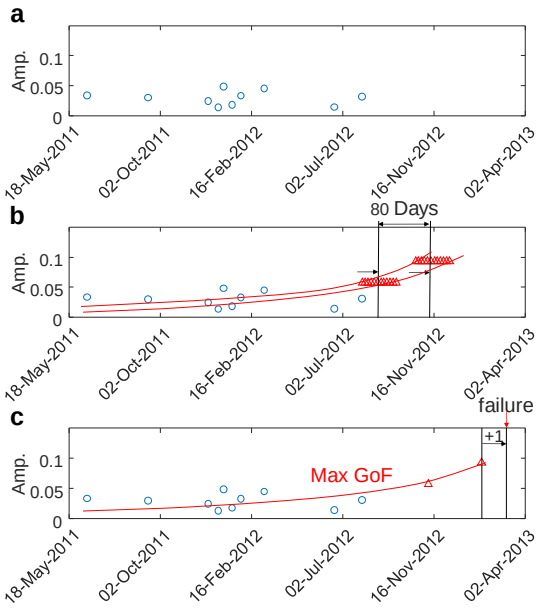

Fig. 11 Overview of the prediction of the failure date: (a) feature extraction, (b) weighted regression, and (c) failure date prediction

The previous studies have limitations that if data of low-level degradation states cover a long period, the regression process may overfit the data in the first part of the period. Therefore, to overcome the limitation, conventional regression techniques are replaced by the following optimization problem (Liu *et al.* 2017)

$$\text{Minimize}_{\alpha,\beta} W = \frac{1}{N}\sum_{i=1}^{N} d_i (f(x_i) - y_i)^2 \quad \text{subject to } f(x_i) = \alpha \times \exp(\beta x_i) \tag{2}$$

where d_i is the weight to compensate for the imbalance of data importance, (x_i, y_i) are the training data points, and α and β are the unknown parameters of the exponential model to optimize, respectively. The pulverizer data given by the PHMAP 2017 Data Challenge is highly imbalanced since it has only two failure-related data (Failure 1 and 2). In addition, the fault features does not increase significantly in the first part as can be seen in Fig. 9. Thus, weighted regression was used to compensate and make the result of the regression model more reasonable.

4.3 Procedures for prediction of failure date

Using the weighted regression algorithm, failure dates were predicted for each testing pulverizer. Fig. 11 shows the procedures used to predict failure dates using the fault features. First, the fault features were extracted from acceleration signals of pulverizers measured at gearbox Case-I, as shown in Fig. 11(a). The features were extracted according to their responses to impact loadings, as described in Section 3.4. Then, the feature values from pulverizers of Failure 1 and 2 (81 and 1 day(s) before

failure) with a distance of 80 days were added after the testing data. The feature values from failure data are marked as red triangles in Fig. 11(b). The goodness-of-fit (GoF) values were calculated using the weighted regression while moving the failure features incrementally starting from the last testing data. Then, the location of the failure data and regression curve was determined when the GoF value was at its maximum, as shown in Fig. 11(c). Finally, the failure date was predicted using the Failure 1 and 2 data.

4.4 Component failure prediction

The faulty component in Pulverizer E was predicted to be Spiral bevel gear A, because peaks of quefrency component in Pulverizer E were coincident with the high shaft component. For prediction of the faulty components in Pulverizers A and B, the high frequency components, in which characteristic behaviors appeared, were investigated. Fig. 12 shows the high frequency components between 2,800 and 3,200 Hz in Pulverizers A and B. As can be seen, the modulated frequency components with 14.8 Hz also appeared, which implied that the high-speed shaft could behave under faulty states. Therefore, the faulty components in Pulverizers A and B were also predicted to be Spiral bevel gear A.

5. Results and discussion

Table 4 shows the predicted failure dates and components; and actual replacement dates and components for the testing Pulverizers A, B, and E. Some of the limitations in the challenge problem could affect the accuracy of the failure prediction method. One of them would be the sparsity of data available for the measurement period. The data measurements were not performed regularly, and the longest gap was about 3 months.

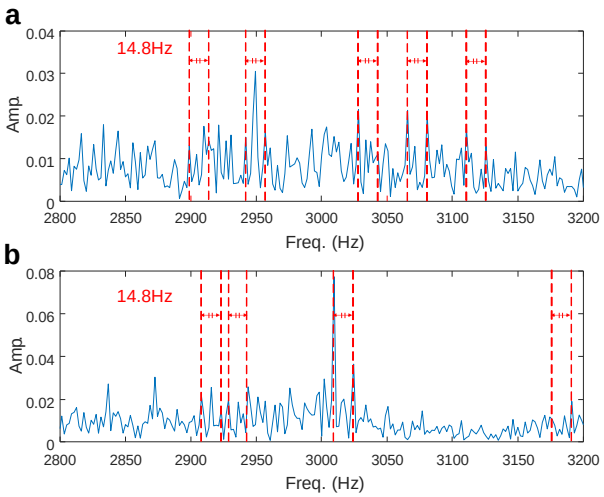

Fig. 12 The behaviors of the high-frequency components in (a) Pulverizer A and (b) Pulverizer B

Table 4 predicted failure dates and components; and actual replacement dates and components for the testing Pulverizers A, B, and E

	Predicted failure date, and component	Actual replacement date, and component
A	2012/12/14, bevel gear A	2012/09/25, bevel gear A
B	2013/12/14, bevel gear A	2014/07/21, bevel gear A
E	2013/12/17, bevel gear A	2013/12/09, bevel gear B

Therefore, it was not clear to observe continuous degradation of the system. In addition, the overall data length was short. In a wind turbine system, vibration signals collected for 10 minutes with 20 kHz are used for condition monitoring (Feng *et al*. 2011). The short data length, along with a low sampling rate, could reduce accuracy of the extracted features (Jung *et al*. 2017). Moreover, the actual replacement dates of the gearboxes could not represent failures of the components. Therefore, these discrepancies between replacements and failures could also affect the accuracy of the results.

6. Conclusions

This paper addresses the prediction method for a failure date prediction of motor-driven gearboxes in pulverizer systems. For that purpose, two fault-related features, HRMS and QA_{HSS} were extracted using frequency response on the high frequency zones and periodical frequency components. Next, the two features were applied to each pulverizer based on frequency response on the impact loadings. Then, a weighted regression algorithm was used with the extracted features to compensate for the imbalance in the degradation data. In addition, predictions for the faulty components were performed based on the modulated behaviors of vibration data in the frequency domain. The prediction results led to the team achieving the highest score in the PHMAP 2017 Data Challenge. However, team SHRMer expects that the accuracy of the prediction method can be improved if the data could be measured more frequently. In addition, a longer measurement time would enhance the reliability of the calculated features. Finally, more details about system configuration and operating conditions could make it possible to extract fault features with more physical meanings.

Acknowledgments

This research is supported in part by OnePredict Inc., conducting Industry-University-Institute Collaborative Research Corporation Support Program from the Commercializations Promotion Agency for R&D Outcomes grant funded by the Ministry of Science, ICT & Future Planning (MSIP) (2016K000377) and in part by the Technology Innovation Program (10050980, System Level

Reliability Assessment and Improvement for New Growth Power Industry Equipment) funded by the Ministry of Trade, Industry & Energy (MI, Korea)..

References

Barszcz, T. and Randall, R.B. (2009), "Application of spectral kurtosis for detection of a tooth crack in the planetary gear of a wind turbine", *Mech. Syst. Signal Pr.*, **23**(4), 1352-1365.

Bogert, B.P., Healy, M.J.R. and Tukey, J.W. (1963), "The quefrency alanysis of time series for echoes: cepstrum, pseudo-autocovariance, cross-cepstrum, and saphe cracking", *Proc. of the Symp. on Time Series Analysis*.

Caselitz, P., Giebhardt, J. and Kewitsch, R. (1999), "Advanced condition monitoring system for wind energy converters", *Proceedings of the EWEC Conference*, Nice, France, March.

Feng, Y., Qiu, Y., Crabtree, C.J., Long, H. and Tavner, P.J. (2011), "Use of SCADA and CMS signals for failure detection and diagnosis of a wind turbine gearbox", *Proceedings of the European Wind Energy Conference and Exhibition 2011*, Brussels, Belgium, March.

Ha, J.M., Youn, B.D., Oh, H., Han, B., Jung, Y. and Park, J. (2016), "Autocorrelation-based time synchronous averaging for condition monitoring of planetary gearboxes in wind turbines", *Mech. Syst. Signal Pr.*, **70**, 161-175.

Hu, C., Youn, B.D., Kim, T. and Wang, P. (2015), "A co-training-based approach for prediction of remaining useful life utilizing both failure and suspension data", *Mech. Syst. Signal Pr.*, **62**, 75-90.

Jung, J.H., Jeon, B.C., Youn, B.D., Kim, M., Kim, D. and Kim, Y. (2017), "Omnidirectional regeneration (ODR) of proximity sensor signals for robust diagnosis of journal bearing systems", *Mech. Syst. Signal Pr.*, **90**, 189-207.

Jung, U. and Koh, B.H. (2014), "Bearing fault detection through multiscale wavelet scalogram-based SPC", *Smart Struct. Syst.*, **14**(3), 377-395.

Lebold, M., McClintic, K., Campbell, R., Byington, C. and Maynard, K. (2000), "Review of vibration analysis methods for gearbox diagnostics and prognostics", *Proceedings of the 54th meeting of the society for machinery failure prevention technology*, Virginia Beach, VA, USA, May.

Li, Y., Ding, K., He, G. and Lin, H. (2016), "Vibration mechanisms of spur gear pair in healthy and fault states" *Mech. Syst. Signal Pr.*, **81**, 183-201.

Liu, J. and Zio, E. (2017), "Weighted-feature and cost-sensitive regression model for component continuous degradation assessment", *Reliab. Eng. Syst. Safe.*, (In press).

McDonald, G.L., Zhao, Q. and Zuo, M.J. (2012), "Maximum correlated Kurtosis deconvolution and application on gear tooth chip fault detection", *Mech. Syst. Signal Pr.*, **33**, 237-255.

McFadden, P.D. (1991), "A technique for calculating the time domain averages of the vibration of the individual planet gears and the sun gear in an epicyclic gearbox", *J. Sound Vib.*, **144**(1), 163-172.

McFadden, P.D. (1994), "Window functions for the calculation of the time domain averages of the vibration of the individual planet gears and sun gear in an epicyclic gearbox", *Transactions-american society of mechanical engineers journal of vibration and acoustics*, **116**(2), 179-187.

Park, J., Ha, J.M., Oh, H., Youn, B.D., Choi, J.H. and Kim, N.H. (2016), "Model-based fault diagnosis of a planetary gear: A novel approach using transmission error", *IEEE T. Reliab.*, **65**(4), 1830-1841.

PHMAP 2017 Data Challenge (2017), http://phmap.org/program/index.kin?gubun=1&sgubun=7

Qu, Y., He, D., Yoon, J., Van Hecke, B., Bechhoefer, E. and Zhu, J. (2014), "Gearbox tooth cut fault diagnostics using acoustic emission and vibration sensors--a comparative study", *Sensors*, **14**(1), 1372-1393.

Randall, R.B. (2016), "A history of cepstrum analysis and its application to mechanical problems" *Mech. Syst. Signal Pr.*, **97**, 3-19

Saxena, A., Wu, B. and Vachtsevanos, G. (2005), "A methodology for analyzing vibration data from planetary gear systems using complex Morlet wavelets", *Proceedings of the American Control Conference*, Portland, OR, USA, June.

Shen, C., Wang, D., Liu, Y., Kong, F. and Tse, P.W. (2014). "Recognition of rolling bearing fault patterns and sizes based on two-layer support vector regression machines", *Smart Struct. Syst.*, **13**(3), 453-471.

Verbruggen, T.W. (2003), "Wind turbine operation & maintenance based on condition monitoring WT-Ω", Project No. 7.4028; ECN Wind Energy

Wei, P., Lu, Z. and Song, J. (2015), "Variable importance analysis: a comprehensive review", *Reliab. Eng. Syst. Safe.*, **142**, 399-432.

Weixun, M. and Tiejun, Z. (2013), "DTM350/600-type Pulverizer driver vibration Fault Cause Analysis and Treatment", *National thermal power 300mw class unit energy efficiency standards and competition annual meeting* (in Chinese).

Yoon, J., He, D. and Van Hecke, B. (2015), "On the use of a single piezoelectric strain sensor for wind turbine planetary gearbox fault diagnosis", *IEEE T. Ind. Electron.*, **62**(10), 6585-6593.

Zhu, D., Feng, Y., Chen, Q. and Cai, J. (2010), "Image recognition technology in rotating machinery fault diagnosis based on artificial immune", *Smart Struct. Syst.*, **6**(4), 389-403.